Solid State Sciences 132 (2022) 106995

Contents lists available at ScienceDirect

Solid State Sciences

journal homepage: www.elsevier.com/locate/ssscie

Flux crystal growth of rubidium–iron silicates and germanates and their ion-exchange using alkali nitrate salts

Mohammad Usman [a], Matthew S. Christian [b], Gregory Morrison [a], Mark D. Smith [a], Weiguo Zhang [c], Theodore M. Besmann [b], P. Shiv Halasyamani [c], Hans-Conrad zur Loye [a,*]

[a] Department of Chemistry and Biochemistry, University of South Carolina, Columbia, SC, 29208, United States
[b] Nuclear Engineering Program, University of South Carolina, Columbia, SC, 29208, United States
[c] Department of Chemistry, University of Houston, Houston, TX, 77204, United States

ARTICLE INFO

Keywords:
Single crystal growth
Ion exchange
Crystal structure
Synthesis

ABSTRACT

Single crystals of two new rubidium ferrites, $RbFeSiO_4$ and $RbFeGeO_4$, were grown out of a eutectic RbCl–RbF melt. Both compounds crystallize in the noncentrosymmetric orthorhombic space group *Ima*2 and exhibit a three-dimensional porous framework structure composed of statistically disordered $(Fe/T)O_4$ (T = Si, Ge) tetrahedra that corner-share to generate large channels running down the *c*-axis. These channels are occupied by Rb ions to maintain charge balance. $RbFeSiO_4$ can also be prepared via a solid-state reaction by mixing and heating stoichiometric amounts of Rb_2CO_3, Fe_2O_3 and elemental Si; however, a similar approach for preparing $RbFeGeO_4$ yielded a mixture of $RbFeGeO_4$ and $RbFeGe_2O_6$. Powder second harmonic generation (SHG) measurements of $RbFeSiO_4$ determined that the material is SHG-active with an intensity of 0.5 times of α-SiO_2. First principles calculations in the form of density-functional theory indicated that it would be possible to ion exchange the Rb cation for other alkali metal cations. Applying a molten alkali nitrate salt-bath treatment at low soak temperatures of 350 °C–450 °C and short soak times of ~16 h resulted in the almost complete replacement of rubidium with potassium and the partial replacement of rubidium with cesium, yielding $K_{0.92}Rb_{0.08}FeSiO_4$, $K_{0.91}Rb_{0.09}FeGeO_4$, and $Cs_{0.48}Rb_{0.52}FeGeO_4$. No ion-exchange was observed when $RbFeSiO_4$ was soaked in molten $CsNO_3$; however, it was possible to force the exchange by using a CsCl melt at 680 °C to yield $Cs_{0.13}Rb_{0.87}FeSiO_4$.

1. Introduction

Complex iron oxides, known as ferrites, have been extensively studied for their electronic and magnetic properties, including ferroelectricity and ferromagnetism [1–6]. In addition, iron-based aluminosilicate-type compounds for ion-exchange applications, albeit rare, are also known [7–9]. Zeolitic type ferro-silicates and germanates contain iron in tetrahedral coordination and form complex framework structures due to the propensity of these elements to assemble as corner-sharing tetrahedra that give rise to three-dimensional porous frameworks capable of hosting a large variety of molecules, ions, and ionic salt lattices [10,11].

Our group has used exploratory flux crystal growth to probe and crystallize new compounds and structure types. Different classes of materials can be grown using different types of fluxes, including metal halides, carbonates, hydroxides, and oxides [12,13]. Alkali halide melts are known to be very efficient in stabilizing tetrahedral iron species, and readily crystallize ferro-silicates and germanates. Very few rubidium silicon, and no rubidium germanium, ferrites are known and they include a rubidium feldspar, $Rb(Fe_{1.1}Si_{2.9})O_8$ [14], and a rubidium leucite, $RbFeSi_2O_6$ [15]. To target the crystallization of additional ferro-silicate and germanate compositions, we utilized eutectic chloride-fluoride fluxes that can dissolve many oxide species and promote low temperature crystal growth. At times, these melts can function as "reactive fluxes" whereby a flux component gets incorporated into the final crystal lattice.

Herein, we report the flux growth synthesis of $RbFeSiO_4$ and the first quaternary rubidium germanium ferrite, $RbFeGeO_4$. We also highlight the solid-state synthesis for $RbFeSiO_4$ using elemental Si, an unconventional Si source in high-temperature solid-state reactions. First principles density-functional theory (DFT) calculations were performed to determine the alkali ion-exchange enthalpies for alkali metal

* Corresponding author.
E-mail address: zurloye@mailbox.sc.edu (H.-C. zur Loye).

https://doi.org/10.1016/j.solidstatesciences.2022.106995
Received 8 July 2022; Received in revised form 8 August 2022; Accepted 10 August 2022
Available online 27 August 2022

analogues of $RbFeTO_4$. This ion-exchange can be achieved by soaking the parent compounds in molten nitrates at about 50 °C above the melting point of the salt. This process is not destructive and was used for single-crystal to single-crystal conversions of $RbFeSiO_4$ to $K_{0.92}Rb_{0.08}FeSiO_4$, and of $RbFeGeO_4$ to $K_{0.91}Rb_{0.09}FeGeO_4$ and $Cs_{0.48}Rb_{0.52}FeGeO_4$. Slightly harsher ion-exchange conditions were used for exchanging Rb in $RbFeSiO_4$ with Cs by soaking it in molten CsCl at 680 °C which led to a 13% Rb exchange with Cs and afforded $Cs_{0.13}Rb_{0.87}FeSiO_4$. An overall illustration of the compounds reported herein and their syntheses and interconversions assisted by molten nitrate salts is provided in Scheme 1.

2. Experimental section

2.1. Reagents

FeF_3 (99%, Strem), Fe_2O_3 (99.5%, Alfa Aesar), SiO_2 (99.9%, Alfa Aesar), GeO_2 (99.999%, Alfa Aesar), Si powder (99.5%, Alfa Aesar), Ge powder (99.999%, Cerac), KNO_3 (99.995%, Alfa Aesar), $CsNO_3$ (99.8%, Alfa Aesar), RbCl (99.8%, Alfa Aesar) and RbF (99.1%, Alfa Aesar) were used as received for all flux growth and solid-state experiments.

2.2. Flux crystal growth and molten nitrate salt bath-assisted ion-exchange

Single crystals of $RbFeTO_4$ were grown by charging a 7.5 cm tall by 1.2 cm diameter silver crucible with FeF_3 as the iron precursor, appropriate TO_2, and RbCl–RbF flux. The silver crucible was crimped shut and the charge was heated in a programmable furnace to 875 °C at a heating rate of 10 °C/min and held at this temperature for 12 h. Subsequently the reactions were slow cooled at 0.1 °C/min to 400 °C, whereupon the furnace was turned off.

Ion-exchange reactions were performed using $RbFeSiO_4$ and $RbFeGeO_4$ by layering 0.1 g of each sample under 1 g of the appropriate nitrate salt in a fused-silica ampule measuring 7.5 cm in length. For ion-exchange involving CsCl, a silver crucible was used as the reaction vessel. The tube containing the charge was heated for 16 h. Post reaction the flux was dissolved in hot water and the crystals were thoroughly rinsed with acetone and examined by single crystal X-ray diffraction. The specific amounts of the reagents and the flux used for the synthesis of all title compositions, in addition to the heating and cooling cycle, are given in Table 1.

2.3. Solid state synthesis

Polycrystalline samples of $RbFeSiO_4$ were synthesized by heating Rb_2CO_3, Fe_2O_3, and elemental Si powder in a stoichiometric ratio. The starting materials were thoroughly mixed in an agate mortar and pestle and then loaded into an alumina crucible that, prior to use, was thoroughly cleaned in aqua regia and dried in a drying oven. The charge was heated at 600 °C/h to 400 °C, maintained at this temperature for 16 h to decompose the carbonate, and then ramped at 600 °C/h to 650 °C, maintained at this temperature for 16 h whereupon the furnace was shut off and allowed to cool to room temperature. Additional intermittent grindings and heat treatments for 16 h at 900 °C led to the formation of a product consisting entirely of the desired compound, $RbFeSiO_4$. One key observation is the necessity of using elemental Si, which afforded only $RbFeSiO_4$, whereas the use of SiO_2 inevitably led to the formation of a small amount of a side product, $RbFeSi_2O_6$, in addition to $RbFeSiO_4$. Similar undesired side products were observed in the case of previously reported $CsFeGeO_4$ [11]. For $RbFeGeO_4$, whether elemental Ge or GeO_2 is used as the Ge source, the formation of undesired $RbFeGe_2O_6$ could not be avoided. PXRD patterns are shown in Figs. S2 and S3.

Table 1
Reagents and reaction conditions for all title compounds.

Composition	Reagents	Flux	Temperature profile
$RbFeSiO_4$	1 mmol FeF_3 1 mmol SiO_2	1.33 g RbCl 0.94 g RbF	Heated at 10 °C/min to 875 °C, held for 12 h and slow cooled to 400 °C at 0.1 °C/min
$RbFeGeO_4$	1 mmol FeF_3 1 mmol GeO_2	1.33 g RbCl 0.94 g RbF	Heated at 10 °C/min to 875 °C, held for 12 h and slow cooled to 400 °C at 0.1 °C/min
$K_{0.92}Rb_{0.08}FeSiO_4$	0.1 g of $RbFeSiO_4$	1 g KNO_3	Heated at 10 °C/min to 350 °C, held for 16 h and shut off
$Cs_{0.13}Rb_{0.87}FeSiO_4$	0.1 g of $RbFeSiO_4$	1 g CsCl	Heated at 10 °C/min to 675 °C, held for 16 h and shut off
$K_{0.91}Rb_{0.09}FeGeO_4$	0.1 g of $RbFeGeO_4$	1 g of KNO_3	Heated at 10 °C/min to 350 °C, held for 16 h and shut off
$Cs_{0.48}Rb_{0.52}FeGeO_4$	0.1 g of $RbFeGeO_4$	1 g of $CsNO_3$	Heated at 10 °C/min to 450 °C, held for 16 h and shut off

2.4. Single crystal X-ray diffraction (SCXRD)

X-ray intensity data from suitable crystals of all reported phases were collected at 301(2) K using a Bruker D8 QUEST diffractometer equipped with a PHOTON 100 CMOS area detector and an Incoatec microfocus source (Mo Kα radiation, $\lambda = 0.71073$ Å) [16]. The raw area detector data frames were reduced and corrected for absorption effects using the SAINT+ and SADABS programs [16,17]. Initial structural models were obtained with SHELXT [18]. Subsequent difference Fourier calculations and full-matrix least-squares refinement against F^2 were performed with

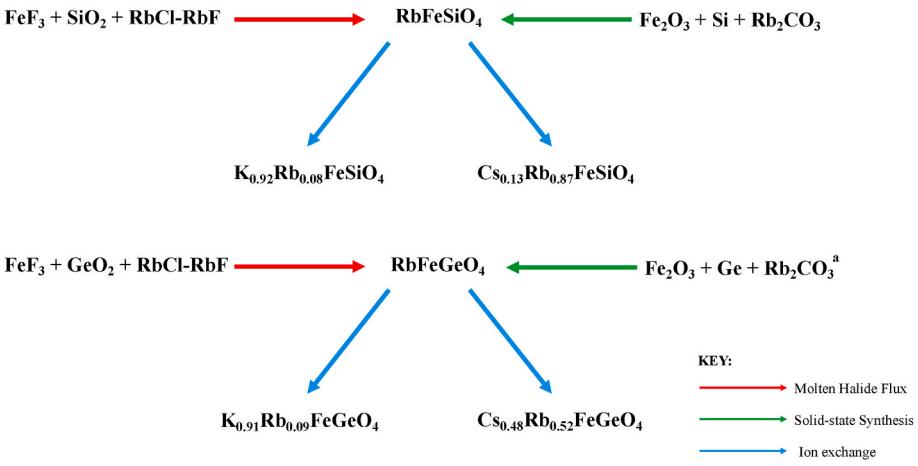

Scheme 1. Illustration of the Synthetic Routes for All Title Compounds.

SHELXL-2018 using the ShelXle interface [19]. Crystallographic and refinement data and interatomic distances for all compounds are listed in Table 2. Additional crystallographic details are provided in the Supporting Information (SI).

2.5. Powder X-ray diffraction (PXRD)

Phase purity of $RbFeSiO_4$ used for bulk property measurements was determined using a Bruker D2 Phaser equipped with an LYNXEYE silicon strip detector and Cu Kα radiation (Cu Kα radiation, $\lambda = 1.5418$ Å). The step-scan covered the angular range 10–70° in steps of 0.02°. The experimental and calculated powder patterns are provided in the SI.

2.6. Energy dispersive spectroscopy (EDS)

Semi-quantitative elemental analyses for all title compounds were carried out using a TESCAN Vega-3 SBU scanning electron microscope (SEM) with EDS capabilities. The crystals were mounted on carbon tape and the analysis was carried out using a 20-kV accelerating voltage and an accumulation time of 20 s. EDS verified the presence of the appropriate elements in all title compositions. Also, the absence of extraneous elements such as silver from the reaction vessel was confirmed within the detection limits of the instrument.

2.7. Optical properties

UV–vis diffuse reflectance spectroscopy data on powder $RbFeSiO_4$ were collected using a PerkinElmer Lambda 35 UV–vis scanning spectrophotometer equipped with an integrating sphere in the range of 300–900 nm. The reflectance data were converted to absorbance data using the Kubelka–Munk function [20].

2.8. Magnetic properties

Magnetic properties for $RbFeSiO_4$ were measured using a Quantum Design Magnetic Properties Measurement System (QD MPMS 3 SQUID Magnetometer). Magnetic susceptibility was measured under zero-field cooled (zfc) and field cooled (fc) conditions from 2 to 300 K in an applied field of 0.1 T. Magnetization as a function of field was measured from – 5 to 5 T at 2 K. Data were corrected for sample shape and radial offset effects as described previously [21]. No differences were observed between the zfc and fc data. Fig. S1 and Table S1.

2.9. Second harmonic generation (SHG)

Powder SHG measurements on polycrystalline $RbFeSiO_4$ were performed on a modified Kurtz nonlinear-optical (NLO) system using a pulsed Nd:YAG laser (Quantel Ultra 50) with a wavelength of 1064 nm. Comparisons with known SHG materials were made using ground crystalline α-SiO_2. A detailed description of the equipment and methodology has been published elsewhere [22,23]. No index-matching material was used in any of the experiments.

2.10. Density-functional theory calculations

Density-functional theory (DFT) optimizations were carried out to calculate K and Cs ion exchange enthalpies. Calculations were performed using the projector-augmented wave (PAW) method as implemented in the Vienna Ab-initio Package (VASP) [24–26] with the Perdew, Burke and Ernzerhof (PBE) exchange-correlation functional [27]. Each calculation used "cold" smearing [28] with a parameter of 0.2 eV and a plane-wave cut-off of 800 eV. In order to properly localize Fe's electrons, a Hubbard U correction [29] of 4.00 eV was specified. Convergence for energy and force were set to 1×10^{-4} eV and 1×10^{-3} eV/Å.

Special quasi-random structures were created to model the partial occupancies of the studied compounds. For the reaction compounds $RbFeGeO_4$ and $RbFeSiO_4$, four structural variations were considered using mixed Fe/Ge and Fe/Si sites. Each of these calculations used $6 \times 5 \times 9$ k-point mesh. Pure K and Cs compounds were modeled as product crystals in order to simplify computations of these crystals and are acceptable as our target is to approximate alkali ion-exchange. $KFeGeO_4$ was modeled with two structures of alternating Fe/Ge layers and three structures with semi-random Fe/Ge sites and used a $5 \times 9 \times 3$ k-point mesh. Three structures converged for $CsFeGeO_4$, which had alternating Fe/Ge layers along either the crystal a, b and c axis, using a $5 \times 5 \times 9$ k-point structures. The large size of the $KFeSiO_4$ cell restricted the number of structures to be considered, so three layered structures were considered, each with alternating Fe and Si layers along the c-axis and using a $3 \times 3 \times 9$ k-point mesh.

The ion exchange energy for element A was calculated using the equation:

$$\Delta H_{ic} = [\Delta H_f(AFeGeO_4) + \Delta H_f(RbX) - \Delta H_f(RbFeGeO_4) - \Delta H_f(AX)]/N$$

where $\Delta H_f(AFeGeO_4)$, $\Delta H_f(RbX)$, $\Delta H_f(RbFeGeO_4)$ and $\Delta H_f(AX)$ are calculated formation enthalpies per N atoms in the crystal cell. DFT formation enthalpies were calculated as:

$$\Delta H_f = E_{DFT} - \sum_{i=1}^{N} \mu_i$$

where E_{DFT} is the calculated DFT energy and μ_i is the atomic chemical potential for species i. Fitted atomic potentials from the Open Quantum

Table 2
Crystallographic and refinement data for all title compounds.

Composition	$RbFeSiO_4$	$RbFeGeO_4$	$K_{0.92}Rb_{0.08}$ $FeSiO_4$	$Cs_{0.13}Rb_{0.87}$ $FeSiO_4$	$K_{0.91}Rb_{0.09}$ $FeGeO_4$	$Cs_{0.52}Rb_{0.48}$ $FeGeO_4$
T (K)	301 (2)					
Crystal setting	Orthorhombic	Orthorhombic	Hexagonal	Orthorhombic	Orthorhombic	Orthorhombic
Space group	*Ima2*	*Ima2*	$P6_3$	*Ima2*	*Pbcm*	*Ima2*
Formula weight	233.41	325.35	190.52	239.68	253.53	300.59
Crystal color and habit	yellow irregular	yellow irregular	orange rod	yellow irregular	orange plate	brown irregular
a (Å)	8.8276(13)	8.9102(3)	18.4330(17)	8.8461(3)	9.1488(10)	9.0979(12)
b (Å)	9.3478(14)	9.3144(3)	18.4330(17)	9.3704(3)	5.5889(6)	9.4660(12)
c (Å)	5.4544(10)	5.6324(2)	8.6158(12)	5.4693(2)	17.2520(18)	5.6615(7)
V (Å^3)	450.09(13)	467.45(3)	2535.2(6)	453.36(3)	882.12(16)	487.57(11)
ρ_{calc} (g/cm^3)	3.445	3.949	2.995	3.512	3.547	4.095
λ (Å)	Mo K_α (0.71073)					
μ (mm^{-1})	14.246	19.767	5.500	13.780	11.790	17.727
Crystal size (mm^3)	0.13 × 0.10 × 0.08	0.08 × 0.03 × 0.02	0.08 × 0.08 × 0.06	0.08 × 0.08 × 0.05	0.14 × 0.08 × 0.06	0.12 × 0.08 × 0.04
Goodness of fit	1.113	1.144	1.076	1.145	1.386	1.268
R_1(I > 2σ(I))	0.0226	0.0291	0.0431	0.0286	0.0559	0.0346
wR_2 (all data)	0.0680	0.0567	0.1110	0.0687	0.1305	0.0759

Materials Database (OQMD) were used for calculation of formation enthalpies [30].

3. Results and discussion

Solid-state syntheses carried out at sufficiently high temperatures are expected to result in thermodynamically stable products, unlike flux reactions that are carried out at lower temperatures and, therefore, can potentially yield kinetically stable (or metastable) phases, which are not obtainable through solid-state techniques. To achieve the crystal growth of complex oxides at lower temperatures, fluoride-chloride fluxes have been used successfully, in part, because of the ability of the fluoride ion to act as a mineralizer and enhance the dissolution of the reagents [12]. Furthermore, the flux can function as a reagent, referred to as a reactive flux, as demonstrated by the synthesis of $RbFeSiO_4$ and $RbFeGeO_4$ grown out of a RbCl–RbF mix, the source of the Rb.

The solid-state synthesis of $RbFeSiO_4$ using SiO_2 failed to result in a phase pure product as inevitably the impurity phase $RbFeSi_2O_6$ formed. We had similar issues attempting to synthesize $CsFeGeO_4$ [11], where we reported that the use of Ge instead of GeO_2 enabled us to obtain a phase pure product. Applying the same approach and using Si instead of SiO_2 as the silicon reagent, we were able to obtain phase pure $RbFeSiO_4$. Extending this synthetic approach to $RbFeGeO_4$, surprisingly failed, and neither elemental Ge nor GeO_2 enabled us to obtain phase pure $RbFeGeO_4$.

Ion-exchange experiments in molten alkali metal nitrates were carried out to prepare additional compositions in the Rb–Fe-T-O phase space. The Fe-T-O framework is stable toward nitrate melts and at the low operating temperatures it is possible to achieve the replacement of one alkali metal for another. This is a "mild" method and soaking $RbFeSiO_4$, for example, in molten KNO_3 at 350 °C results in a single-crystal to single-crystal ion exchange that yielded $K_{0.91}Rb_{0.09}FeSiO_4$ in about 16 h.

3.1. Structures

3.1.1. $RbFeSiO_4$

$RbFeSiO_4$, isostructural with three other compositions reported herein, $RbFeGeO_4$, $Cs_{0.13}Rb_{0.87}$ $FeSiO_4$, and $Cs_{0.52}Rb_{0.48}$ $FeGeO_4$, crystallizes in the polar acentric orthorhombic space group *Ima*2 with lattice parameters $a = 8.8276(13)$ Å, $b = 9.3478(14)$ Å, and $c = 5.4544(10)$ Å. The asymmetric unit consists of one Rb atom, one split (50/50) Fe/Si site, and three O atoms. The Fe/Si site is coordinated to four O atoms with bond lengths 1.715(2) Å to O(1), 1.748(5) Å to O(1), 1.714(2) Å to O(2), and 1.6973(7) Å to O(3), to form $(Fe/Si)O_4$ tetrahedra that corner-share to form $[FeSiO_4]^-$ sheets that are connected to produce voids in which the Rb ions are located. The Rb cations provide charge balance to the overall anionic framework, as depicted in Figs. 1 and 2.

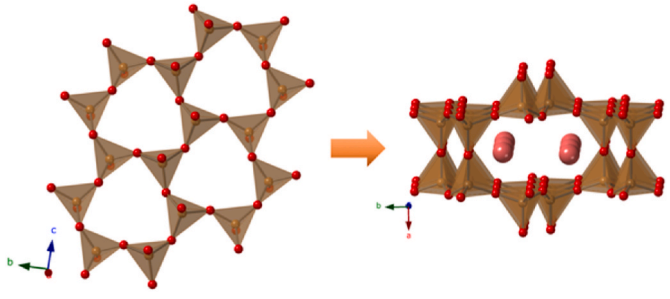

Fig. 1. $(Fe/Si)O_4$ silicate sheet topology in $RbFeSiO_4$ (left of the arrow); connection of these sheets via corner-sharing produces cavities occupied by Rb ions (right of the arrow). Mixed Fe/Si sites are shown in brown, Rb atoms in salmon, and O atoms in red. (For interpretation of the references to color in this figure legend, the reader is referred to the Web version of this article.)

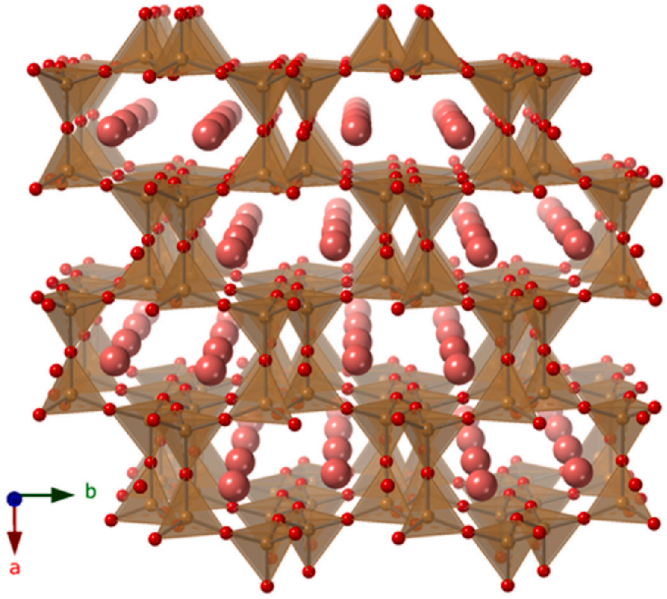

Fig. 2. Polyhedral representation of the $RbFeSiO_4$ crystal structure. Mixed Fe/Si sites are shown in brown, Rb atoms in salmon, and O atoms in red. (For interpretation of the references to color in this figure legend, the reader is referred to the Web version of this article.)

3.1.2. $K_{0.91}Rb_{0.09}FeGeO_4$

$K_{0.91}Rb_{0.09}FeGeO_4$, obtained via ion exchange, crystallizes in the orthorhombic space group *Pbcm* with lattice parameters $a = 9.1488(10)$ Å, $b = 9.3478(14)$ Å, and $c = 17.2520(18)$ Å. The asymmetric unit consists of two split (50/50) Fe/Ge sites, two mixed K/Rb sites, which are predominantly K, and five O atoms. Fe/Ge(1) is coordinated to four O atoms with bond lengths 1.804(5) Å to O(2), 1.803(5) Å to O(3), 1.798 (5) Å to O(3), and 1.798(3) Å to O(5), to form $Fe/Ge(1)O_4$ tetrahedra. Fe/Ge(2) is coordinated to four O atoms with bond lengths 1.792(5) Å to O(1), 1.818(5) Å to O(1), 1.798(5) Å to O(2), and 1.798(3) Å to O(4), to form $Fe/Ge(2)O_4$ tetrahedra. These tetrahedra exclusively corner-share to form a sheet topology similar to the one found in $RbFeSiO_4$, as illustrated in Fig. 3. The $[FeGeO_4]^-$ sheets further connect through corner-sharing to generate a complex three-dimensional porous framework stabilized by disordered K and Rb ions that reside in the channels.

$K_{0.92}Rb_{0.08}FeSiO_4$ crystallizes in the polar acentric hexagonal space group $P6_3$ with lattice parameters $a = 18.4330(17)$ Å and $c = 8.6158$ (12) Å. The asymmetric unit consists of eight statistically disordered Fe/Si sites, six mixed K/Rb sites, and sixteen oxygen atoms. All Fe/Si sites are coordinated to oxygen to form $(Fe/Si)O_4$ tetrahedra that connect via corner-sharing to generate a porous framework that contains channels occupied by clusters of disordered K/Rb ions that maintain charge

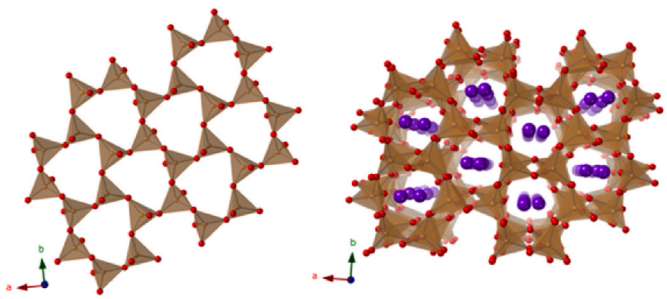

Fig. 3. Sheet topology and crystal structure of $K_{0.91}Rb_{0.09}FeGeO_4$, shown on the left and right, respectively. Mixed Fe/Ge sites are shown in brown, K/Rb sites in purple, and O atoms in red. (For interpretation of the references to color in this figure legend, the reader is referred to the Web version of this article.)

balance. Fig. 4 shows a perspective view of the $K_{0.92}Rb_{0.08}FeSiO_4$ crystal structure.

3.2. DFT results

The formation enthalpies for the calculated structures are listed in Table 3 and detail the lowest, highest and average formation enthalpies of all SQS for each structure. The difference in calculated formation enthalpies for all alkali is small with differences no greater than 0.04 eV/atom. Based on these data one might expect, correctly, that all compositions can be prepared. K and Cs crystals are shown to be more stable than Rb crystals for the Ge structures, while Si structures prefer Rb over K.

Table 4 lists the lowest, highest and average calculated ion-exchange enthalpies between all SQSs. The results show that ion-exchange is possible for all structures and is preferred for the Ge crystals. Though the average ion-exchange energy for Si is positive, thermal effects are not included in these calculations and likely contribute to the stabilization of the ion-exchanged complex. Nonetheless, the fact that some SQS ion-exchange enthalpies are negative provides a favorable probability for the reaction to occur.

Additionally, the largest SQSs ion-exchange enthalpies were calculated when the initial structure contained greater alkali ordering than the final structure indicating that exchange favors random mixing of the alkali atoms. This also indicates that the average exchange enthalpy for $RbFeSiO_4$ is positive likely because the representative SQSs used for our calculations did not adequately capture the random nature of ion-exchange for this system.

Experimentally we observed that performing the ion exchange in a molten alkali nitrate salt-bath treatment resulted in the almost complete replacement of rubidium with potassium and the partial replacement of rubidium with cesium, yielding $K_{0.92}Rb_{0.08}FeSiO_4$, $K_{0.91}Rb_{0.09}FeGeO_4$, and $Cs_{0.48}Rb_{0.52}FeGeO_4$. No ion-exchange was observed when $RbFeSiO_4$ was soaked in molten $CsNO_3$; however, it was possible to force the exchange by using a CsCl melt at 680 °C to yield $Cs_{0.13}Rb_{0.87}FeSiO_4$. By comparison with $CsFeGeO_4$, whose ion exchange behavior we reported previously [11], we found that $CsFeGeO_4$ completely exchanges with potassium forming $KFeGeO_4$ and almost completely with rubidium, forming $Rb_{0.94}Cs_{0.06}FeGeO4$; the reverse of the latter process, the exchange of cesium for rubidium, starting with $RbFeGeO_4$, described in this paper, is incomplete, resulting in $Cs_{0.48}Rb_{0.52}FeGeO_4$. Similarly, the exchange of potassium for rubidium is less complete for $RbFeGeO_4$, resulting in $K_{0.91}Rb_{0.09}FeGeO_4$ rather than pure $KFeGeO_4$ when starting from $CsFeGeO_4$. Overall, however, the molten nitrate ion exchange approach is useful for kinetic stabilization of different phases and can result in a single crystal to single crystal compositional transformation.

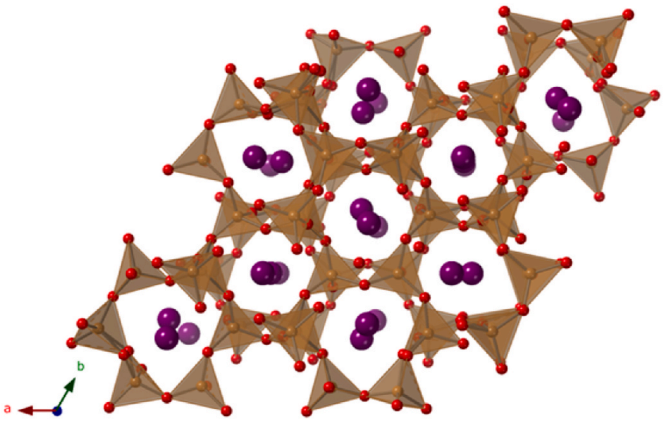

Fig. 4. Perspective view of $K_{0.92}Rb_{0.08}FeSiO_4$ down the *c*-axis. Fe/Si sites are shown in brown, K/Rb sites in purple, and O atoms in red. (For interpretation of the references to color in this figure legend, the reader is referred to the Web version of this article.)

Table 3
Calculated lowest, highest and average formation enthalpies for each complex in eV/atom.

(eV/atom)	Low ΔH_f	High ΔH_f	Avg ΔH_f
$KFeGeO_4$	−1.52	−1.60	−1.56
$RbFeGeO_4$	−1.49	−1.58	−1.54
$CsFeGeO_4$	−1.52	−1.56	−1.55
$KFeSiO_4$	−2.01	−2.02	−2.02
$RbFeSiO_4$	−2.02	−2.09	−2.06

Table 4
Calculated ion-exchange enthalpies in eV/atom.

(eV/atom)	Low ΔH_{ie}	High ΔH_{ie}	Avg ΔH_{ie}
$RbFeGeO_4 \rightarrow KFeGeO_4$	0.0285	−0.1377	−0.0517
$RbFeGeO_4 \rightarrow CsFeGeO_4$	0.0334	−0.0934	−0.0365
$RbFeSiO_4 \rightarrow KFeSiO_4$	0.0281	−0.0504	0.0919

3.3. Optical properties

Materials that crystallize in noncentrosymmetric space groups, with exception to the 432 crystal class, may exhibit SHG property [31]. Large dipole moments are typically associated with high SHG efficiency [32,33]. $RbFeSiO_4$was found to be SHG-active with an intensity equal to 0.5 times that of α-SiO_2 (39.2 a.u. for $RbFeSiO_4$ vs 83.6 a.u. for SiO_2), hence confirming its acentric space group *Ima*2. The low SHG-efficiency could be attributed to a small dipole moment of the material in addition to its yellow-orange appearance.

The UV–vis absorption data for $RbFeSiO_4$ are shown in Fig. 5. The band gap for the compound falls in the range of 1.7–1.8 eV. (700–725 nm), which is consistent with its yellow-orange physical appearance and with the band gaps of the materials that mostly absorb in the blue-indigo (420–490 nm or 2.53–2.95 eV) region of the visible light spectrum. Additionally, the optical band gap for $RbFeSiO_4$ is also in agreement with that of Fe_2O_3 (E_g = ~2.10 eV) [34] and other complex iron-based oxides, all exhibiting red-orange-yellow appearance [35–37].

4. Conclusion

Single crystals of two new rubidium ferrites, $RbFeSiO_4$ and $RbFeGeO_4$, were grown out of a eutectic RbCl–RbF melt and they crystallize

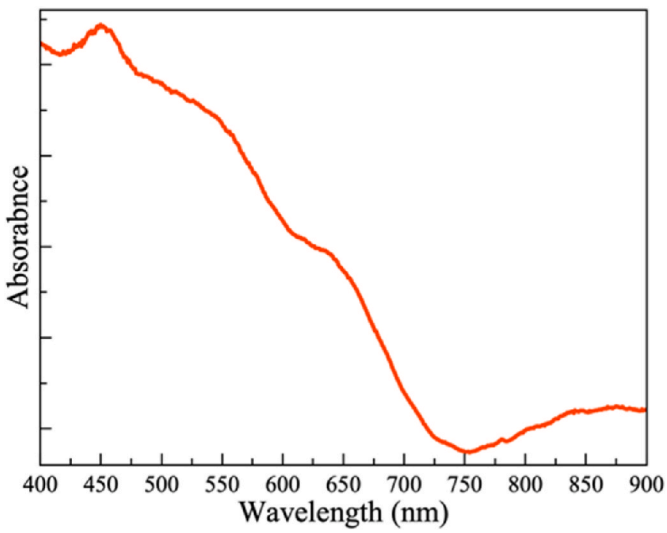

Fig. 5. UV–vis plot for $RbFeSiO_4$.

in a channel containing framework structure. The alkali metals present in the channels can be ion exchanged, to various degrees, in a molten nitrate environment to result in a crystal-to-crystal transformation. DFT calculations indicate the $AFeSiO_4$ and $AFeGeO_4$ (A = K, Rb, Cs) should be stable and that the ion exchange energies are quite small and feasible, in agreement with what was observed experimentally. UVvis spectroscopy measurements on $RbFeSiO_4$ indicated that it is a semiconductor with a bandgap between 1.7 and 1.8 eV.

Credit author statement

Usman – synthesis and characterization, writing Christian – DFT calculations, reviewing Morrison – magnetic measurements and analysis, reviewing Smith – structure determination, reviewing Zhang – SHG measurement, reviewing Besmann – DFT calculation, reviewing Halasyamani – SHG measurement, reviewing, zur Loye - conceptualization, methodology, writing, reviewing.

Accession codes

CCDC 2169184–2169189 contain the supplementary crystallographic data for this paper. These data can be obtained free of charge via www.ccdc.cam.ac.uk/data_request/cif, or by emailing data_request@ccdc.cam.ac.uk, or by contacting The Cambridge Crystallographic Data Centre, 12 Union Road, Cambridge CB2 1EZ, UK; fax: +44 1223 336033.

Declaration of competing interest

The authors declare that they have no known competing financial interests or personal relationships that could have appeared to influence the work reported in this paper.

Acknowledgements

Financial support for this work provided by the National Science Foundation under DMR-1806279 and OIA-655740 is gratefully acknowledged. PSH and WZ thank the Welch Foundation (Grant E-1457) and the NSF-DMR-2002319 for support. Syntheses, structure determination, magnetic measurements, DFT calculations, and ion exchange experiments were performed at UofSC. SHG measurements were performed at the University of Houston.

Appendix A. Supplementary data

Supplementary data to this article can be found online at https://doi.org/10.1016/j.solidstatesciences.2022.106995.

References

[1] C. Delacotte, F. Hue, Y. Breard, S. Hebert, O. Perez, V. Caignaert, J.M. Greneche, D. Pelloquin, Structural transition at 360 K in the $CaFe_5O_7$ ferrite: toward a new charge ordering distribution, Inorg. Chem. 53 (2014) 10171–10177.
[2] N. Hayashi, T. Yamamoto, H. Kageyama, H. Nishi, Y. Watanabe, T. Kawakami, Y. Matsushita, A. Fujimori, M. Takano, $BaFeO_3$: a ferromagnetic oxide, *Angew. Chem., Int. Ed.* 50 (2011) 12547–12550.
[3] G. Catalan, J.F. Scott, Physics and applications of bismuth ferrite, Adv. Mater. 21 (2009) 2463–2485.
[4] W. Eerenstein, N.D. Mathur, J.F. Scott, Multiferroic and magnetoelectric materials, Nature 442 (2006) 759–765.
[5] S.-W. Cheong, M. Mostovoy, Multiferroics: a magnetic twist for ferroelectricity, Nat. Mater. 6 (2007) 13–20.
[6] M.M. Smart, T.M.S. Pellizzeri, G. Morrison, C.D. McMillen, H.-C. zur Loye, J. W. Kolis, Ferrite materials containing kagomé layers: chemistry of $Ba_2Fe_{11}Ge_2O_{22}$ and $K_2Co_4V_9O_{22}$ hexaferrites, Chem. Mater. 33 (7) (2021) 2258–2266.
[7] R.B. Borade, A. Clearfield, Synthesis of an iron silicate with the ferrierite structure, Chem. Commun. 19 (1996) 2267–2268.
[8] P.N. Joshi, S.V. Awate, V.P. Shiralkar, Partial isomorphous substitution of Fe^{3+} in the LTL framework, J. Phys. Chem. 97 (1993) 9749–9753.
[9] D.E.W. Vaughan, K.G. Strohmaier, I.J. Pickering, G.N. George, Transition metal framework substitutions in sodalites, Solid State Ionics 53–56 (1992) 1282–1291.
[10] P.F. Henry, M.T. Weller, CsFeSiO4: a maxium iron content zeotype, Chem. Comm. (1998) 2723–2724.
[11] M. Usman, V. Kocevski, M.D. Smith, G. Morrison, W. Zhang, Halasyamani P. S. Besmann, H.-C. zur Loye, Polymorphism and molten nitrate salt-assisted single crystal to single crystal ion exchange in the cesium ferrogermanate zeotype: $CsFeGeO_4$, Inorg. Chem. 59 (2020) 9699–9709.
[12] D.E. Bugaris, H.-C. zur Loye, Materials discovery by flux crystal growth: quaternary and higher order oxides, Angew. Chem. Int. Ed. 51 (16) (2012) 3780–3811.
[13] V.V. Klepov, C.A. Juillerat, K.A. Pace, G. Morrison, H.-C. zur Loye, Soft" alkali bromide and iodide fluxes for crystal growth, Front. Chem. 8 (2020) 518.
[14] G.D. Brunton, L.A. Harris, O.C. Kopp, Crystal structure of a rubidium iron feldspar, Am. Mineral. 57 (1972) 1720–1728.
[15] A.M. Bell, C.M. Henderson, Rietveld refinement of the structures of dry-synthesized $MFe^{III}Si_2O_6$ leucites (M = K, Rb, Cs) by synchrotron X-ray powder diffraction, Acta Crystallogr. C 50 (10) (1994) 1531–1536.
[16] APEX3 Version 2016.5-0 and SAINT+ Version 8.37A, Bruker AXS, Inc, Madison, Wisconsin, USA, 2016.
[17] SADABS-2016/2: krause, L., herbst-irmer, R., sheldrick G.M. And stalke D, J. Appl. Crystallogr. 48 (2015) 3–10.
[18] (a) SHELXT, G.M. Sheldrick, Acta Crystallogr. A71 (2015) 3–8;
(b) SHELXL, G.M. Sheldrick, Acta Crystallogr. C71 (2015) 3–8.
[19] C.B. Hübschle, G.M. Sheldrick, B. Bittrich, ShelXle: a Qt graphical user interface for SHELXL, J. Appl. Crystallogr. 44 (2011) 1281–1284.
[20] P. Kubelka, F. Munk, Ein Beitrag zur Optik der Farbanstriche, Z. Technol. Phys. 12 (1931) 593.
[21] G. Morrison, H.-C. zur Loye, Simple correction for the sample shape and radial offset effects on SQUID magnetometers: magnetic measurements on Ln_2O_3 (ln = Gd, Dy, Er) standards, J. Solid State Chem. 221 (2015) 334–337.
[22] S.K. Kurtz, T.T. Perry, A powder technique for the evaluation of nonlinear optical materials, J. Appl. Phys. 39 (1968) 3798.
[23] D. Schlüter, H. Müller-Buschbaum, Eine perowskitstaplevariante mit geordneter metallverteilung: $Ba_6Al_2Rh_2Ho_2O_{15}$, J. Alloys Compd. 191 (1993) 305–308.
[24] G. Kresse, Efficient iterative schemes for Ab initio total-energy calculations using a plane-wave basis set, Phys. Rev. B 54 (16) (1996) 11169–11186.
[25] G. Kresse, J. Hafner, Ab initio molecular-dynamics simulation of the liquid-metalamorphous- semiconductor transition in germanium, Phys. Rev. B 49 (20) (1994) 14251–14269.
[26] G. Kresse, J. Hafner, Ab initio molecular dynamics for liquid metals, Phys. Rev. B 47 (1) (1993) 558–561.
[27] J. Perdew, K. Burke, M. Ernzerhof, Generalized gradient approximation made simple, Phys. Rev. Lett. 77 (18) (1996) 3865–3868.
[28] N. Marzari, D. Vanderbilt, A. de Vita, M.C. Payne, Thermal contraction and disordering of the Al(110), Surface 110 (1999) 4.
[29] M. Cococcioni, The LDA+U Approach: A Simple Hubbard Correction for Correlated Ground States, vol. 2, 2012.
[30] S. Kirklin, J.E. Saal, B. Meredig, A. Thompson, J.W. Doak, M. Aykol, S. Rühl, C. Wolverton, The open Quantum materials Database (OQMD): assessing the accuracy of DFT formation energies, npj Computational Materials 1 (October) (2015).
[31] S.-H. Kim, J. Yeon, P.S. Halasyamani, Noncentrosymmetric polar oxide material, Pb_3SeO_5: synthesis, characterization, electronic structure calculations, and structure-property relationships, Chem. Mater. 21 (2009) 5335–5342.
[32] S.D. Nguyen, J. Yeon, S.-H. Kim, P.S. Halasyamani, $BiO(IO_3)$: a new polar iodate that exhibits an aurivillius-type $(Bi_2O_2)^{2+}$ layer and a large SHG response, J. Am. Chem. Soc. 133 (2011) 12422–12425.
[33] J. Yeon, S.-H. Kim, S.D. Nguyen, H. Lee, P.S. Halasyamani, Two new noncentrosymmetric (NCS) polar oxides: syntheses, characterization, and structure-property relationships in $BaMTe_2O_7$ ($M = Mg^{2+}$ or Zn^{2+}), Inorg. Chem. 51 (2012) 2662–2668.
[34] C. Xia, Y. Jia, M. Tao, Q. Zhang, Tuning the band gap of hematite α-Fe_2O_3 by sulfur doping, Phys. Lett. 377 (2013) 1943––1947.
[35] Q.U. Hassan, D. Yang, J.P. Zhou, Y.X. Lei, J.Z. Wang, S.U. Awan, Novel single-crystal hollandite $K_{1.46}Fe_{0.8}Ti_{7.2}O_{16}$ microrods: synthesis, double absorption, and magnetism, Inorg. Chem. 57 (2018) 15187–15197.
[36] M. Usman, V. Kocevski, M.D. Smith, G. Morrison, T. Besmann, H.-C. zur Loye, New rubidium-containing mixed-metal titanium hollandites, Cryst. Growth Des. 20 (4) (2020) 2398–2405.
[37] Z.-Q. Guo, N.-X. Miao, J.-P. Zhou, Y.-X. Lei, Q.U. Hassan, M.-M. Zhou, Novel magnetic semiconductor $Na_2Fe_2Ti_6O_{16}$: synthesis, double absorption and strong adsorptive ability, J. Mater. Chem. 5 (2017) 17589–17600.